Turkish Journal of Physics

http://journals.tubitak.gov.tr/physics/

Invited Research Article

Turk J Phys
(2014) 38: 442 – 449

doi:10.3906/fiz-1405-1

The influence of TiO_2 nanostructure properties on the performance of TiO_2-based anodes in lithium ion battery applications

Xiang LIU[1], Qian SUN[1], Fangzhou LIU[1], Aleksandra B. DJURIŠIĆ[1,*], Alan Man Ching NG[2], Maohai XIE[1], Tom WOOD[3], Juan Antonio ZAPIEN[3], Changzhong LIAO[4], Kaimin SHIH[4]

[1]Department of Physics, University of Hong Kong, Pokfulam Road, Hong Kong
[2]Department of Physics, South University of Science and Technology of China, Shenzhen, China
[3]Department of Physics and Materials Science, City University of Hong Kong, Kowloon Tong, Hong Kong
[4]Department of Civil Engineering, University of Hong Kong, Pokfulam Road, Hong Kong

Received: 05.05.2014 • **Accepted:** 20.05.2014 • **Published Online:** 10.11.2014 • **Printed:** 28.11.2014

Abstract: We investigated the properties of 7 different titanium dioxide nanostructures with different crystal structures (3 anatase, 2 rutile, and 2 mixed anatase–rutile phase). Nanoparticle samples and mesoporous sphere samples were investigated. Even for the same crystal structure, significant variations in performance were observed for anatase titania samples, while 2 rutile samples exhibited similar performance inferior to anatase-based anodes. Mixed-phase samples also exhibited lower specific capacity compared to the best performing anatase samples, and in this case a significant difference in performance was observed between nanoparticles and mesoporous spheres.

Key words: Lithium ion battery, titanium dioxide

1. Introduction

Titanium dioxide is a material of significant interest for lithium ion battery (LIB) applications [1–22]. Compared to conventionally used graphite anode, TiO_2 would result in significant improvements in battery safety due to its higher operating voltage, which affects the formation of the solid-electrolyte interface (SEI) layer and prevents the formation of metallic lithium dendrite structures [1,4]. The theoretical capacity of titania ($\sim$335 mA h/g) is comparable to that of graphite ($\sim$372 mA h/g) [1,4], while it also exhibits a small volume expansion upon lithium insertion/extraction ($\sim$4% for anatase) [1]. Therefore, TiO_2-based anodes for LIB applications have been extensively studied [1–22]. These studies include different morphologies of titania as well as different crystal structures, and combinations of titania with other materials to enhance cycling and rate performance [20–22].

The main drawbacks of titania-based anodes are low Li-ion diffusivity and low electronic conductivity, which limit the rate performance [1,20]. The insertion/extraction of Li^+ into titania can be described with the following equation:

$$xLi^+ + TiO_2 + xe^- \leftrightarrow Li_xTiO_2, \tag{1}$$

where x is between 0 and 1, depending on the crystal structure of TiO_2 [1]. In the case of bulk rutile, lithium capacity is very low, but it can be increased with rutile nanocrystals [1,4]. Nanostructuring of the anatase can

*Correspondence: dalek@hku.hk

also help improve its lithium capacity, while brookite titania is considered to have the best potential for lithium insertion/extraction due to its more open structure [1]. Nanostructuring in general is a well-recognized strategy for improving the lithium storage capacity of titania [1–3]. However, despite the known effects of the morphology and crystal structure, systematic studies of the effects of these parameters on the performance of titania-based anodes in LIBs have been scarce [1]. Furthermore, a very wide range of cycling and/or rate performances of commercial titania samples has been reported in the literature, with initial specific capacities ranging from below 75 mA h/g [12] to over 270 mA h/g [11]. Such large disparity in the performance of commercial samples is likely not only due to differences in sizes and possibly crystal structures, but also differences in native defects since the native defects have a strong influence on the properties of metal oxides.

To shed some light, we investigated the influence of titania nanoparticle properties on their performance in LIB applications. To facilitate our investigation, we selected nanoparticle samples from different commercial sources, including samples with different crystal structures (anatase, rutile, or a mixture of them). In addition to commercial nanoparticles, we also prepared mesoporous titania spheres [23]. Among different titania morphologies, mesoporous structures are considered to be particularly promising for LIB applications [1,3,5]. This is due to a large electrode/electrolyte interface area, as well as short lithium diffusion paths [5]. All the samples were comprehensively characterized using electron microscopy, X-ray diffraction, and Raman spectroscopy, and their performance in LIB applications was evaluated. Obtained results are discussed in detail.

2. Experimental details

2.1. Material synthesis

TiO_2 nanoparticles were purchased from different suppliers. Three samples of anatase TiO_2 were obtained from Nanostructured & Amorphous Materials, Inc. (99%, average particle size (APS): 15 nm), MK Impex Corp. (95%, APS: 7 nm), and SkySpring Nanomaterials, Inc. (99.5%, APS: 10-30 nm), and were labeled as A-NA, A-MK, and A-SKS, respectively. Two rutile TiO_2 nanoparticle samples were purchased from Nanostructured & Amorphous Materials, Inc. ($>$98%, Diameter: 10 nm and length: 40 nm) and MK Impex Corp. (99%, APS: 50 nm), and labeled as R-NA and R-MK, respectively. Aeroxide TiO_2 P25 (99.5%, APS: 21 nm) nanoparticles were obtained from Sigma-Aldrich, and labeled as P25. Tetrabutyl titanate (TBT) (97%) and concentrated sulfuric acid (95.0%–98.0%) were purchased from Sigma-Aldrich. All the chemicals were used without any further purification.

A hydrothermal method was used for the synthesis of TiO_2 microspheres according to previously reported procedures [23]. Briefly, 0.5 mL of TBT was added to 30 mL of 2 M sulfuric acid aqueous solution and stirred for 30 min. Then the solution was transferred into a Teflon-lined stainless steel autoclave (Parr Instrument Company), and the autoclave was placed in an oven at 180 °C for 24 h. Then the autoclave was cooled down to room temperature and the product was washed with deionized water and collected. Finally the TiO_2 microsphere powders were annealed at 450 °C for 30 min, and the obtained sample was labeled as sphere.

2.2. Characterization

A Bruker D8 advance diffractometer using Cu Kα radiation ($\lambda = 0.154184$ nm) was employed for collecting the X-ray diffraction (XRD) patterns of the samples ($2\theta = 20 - 80^{\circ}$). The morphologies of different electrodes were examined by scanning electron microscopy (SEM) using a JEOL JMS-7001F System, and the Raman spectra were obtained by Renishaw Raman Spectroscopy 2000 system.

2.3. Electrochemical measurements

Electrochemical measurements were conducted using a coin-cell (CR2032) with lithium metal (15.6 mm in diameter, 0.25 mm in thickness) as a counter-electrode. For anode preparation, titania samples were mixed with the conductive carbon additives (carbon black, Super-P@Li, Timcal) and binder (polyvinylidene fluoride, PVDF, MTI) in a weight ratio of 80:10:10. The mixture was dried in vacuum at 90 °C for 12 h and then the viscosity was adjusted with NMP solvent and the resulting slurry was coated on copper foil substrates by doctor blading. After coating and drying, electrodes were cut into 14-mm-diameter disks. Cells were assembled in an Ar-filled glove box. The electrolyte, which consisted of 1 M $LiPF_6$ in a 1:1:1 (in volume) mixture of ethylene carbonate (EC)/dimethyl carbonate (DMC)/diethyl carbonate (DEC), was purchased from MTI Corporation. The galvanostatic charge/discharge cycles were tested with a Neware BTS3000 battery test system at various current densities of 100 mA $g^{-1} \sim 1$ A g^{-1} between 3.0 and 1.0 V. The specific capacities were calculated on the basis of the total weight of the active materials.

3. Results and discussion

Figure 1 shows the SEM images of different titania samples. Good agreement is observed between the nanoparticle morphology, APS, observed and the specifications provided by the commercial supplier, as summarized in the Table. Compared to nanoparticles, mesoporous titania microspheres exhibit significantly larger size. To obtain more information about the samples, X-ray diffraction measurements were performed, and the obtained results are shown in Figure 2. The crystallite sizes obtained from XRD data [24] are also summarized in the Table. It can be observed that one of the nanoparticle samples, which is expected to be anatase, namely A-SKS, also shows the diffraction peaks corresponding to a rutile phase. In addition, R-MK particles also show a small contribution from an anatase phase. More significant presences of both anatase and rutile phases are observed as expected in P25 samples, as well as in titania microspheres.

Table. Morphology and crystallinity parameters of different TiO_2 samples.[a]

Sample	Anatase (nm)	Rutile (nm)	APS (nm)
A-NA	6	–	15
A-MK	5	–	7
A-SKS	16	22	10–30
R-NA	–	8	10, 40
R-MK	–	17	50
P25	19	34	21
Sphere	18	10	4300

[a] APS (average particle size) of the spheres was determined by SEM, while for the nanoparticles, the information from the suppliers were used. The crystal size was calculated by using the double-Voigt approach [24], which was implemented in TOPAS4.2 software.

The electrochemical performance of different titania anodes was evaluated and the obtained results are shown in Figures 3 and 4, respectively. For A-NA samples, we can observe a significant decrease in the performance, from initial specific capacity of 236 mA h/g to 184 mA h/g in the second cycle, followed by a further decrease to 92 mA h/g in the 50th cycle and 59 mA h/g in the 80th cycle. The capacity at 0.1 A/g charge/discharge rate was 155 mA h/g, which was reduced to 101 mAh/g at 1A/g rate, followed by a recovery to 146 mA h/g when charge/discharge rate is again reduced to 0.1 A/g. A-MK samples exhibit significantly

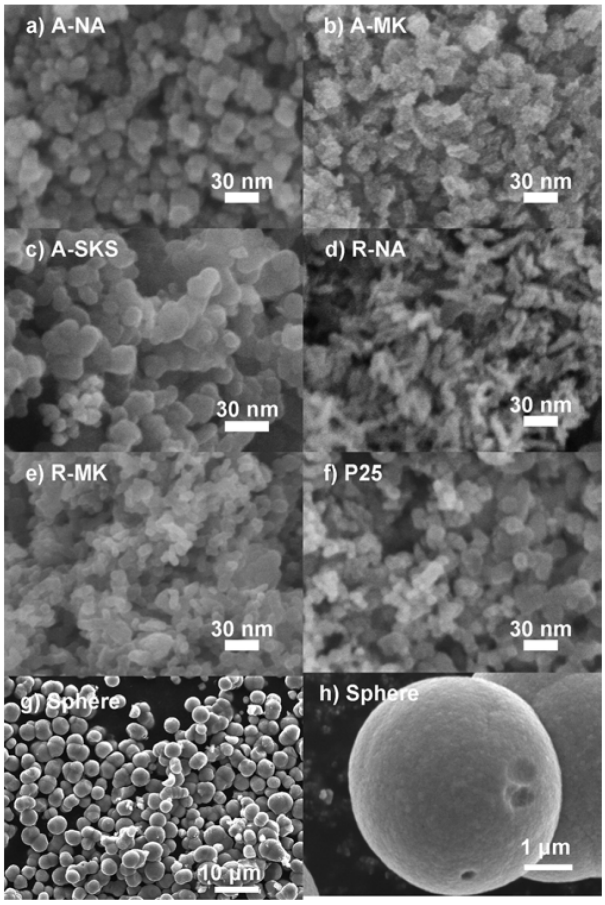

Figure 1. SEM images of different TiO_2 samples: (a) A-NA; (b) A-MK; (c) A-SKS; (d) R-NA; (e) R-MK; (f) P25; (g, h) TiO_2 microsphere.

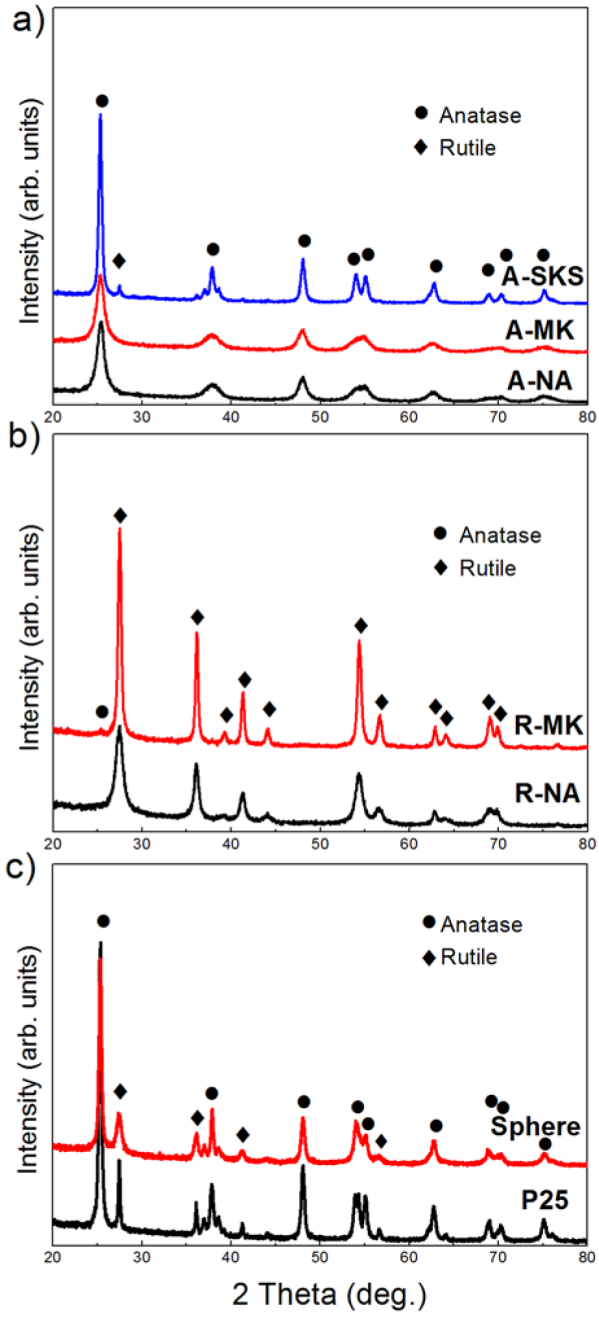

Figure 2. XRD patterns of different TiO_2 samples. (a) A-NA, A-MK, and A-SKS; (b) R-NA and R-MK; (c) P25 and TiO_2 microsphere. The peaks have been indexed according to JCPDS 04-0477 for anatase TiO_2 and JCPDS 04-0551 for rutile TiO_2.

better cycling and rate performance, with the drop of initial capacity from 230 mA h/g to 176 mAh/g in the second cycle, and maintaining a stable capacity in the range 156–160 mA h/g from the 10th to the 80th cycle. In terms of the rate performance, obtained specific capacities following rate changes from 0.1 A/g to 1 A/g and back to 0.1 A/g were 167 mA h/g, 133 mA h/g, and 164 mA h/g. A-SKS sample exhibited better cycling performance compared to A-NA with the specific capacity drop from 186 mA h/g (initial) to 158 mA h/g (second cycle) and 139 mA h/g (80th cycle). However, the rate performance of this sample was inferior, with specific capacity of 96 mA h/g at the charge/discharge rate of 1 A/g. The inferior rate performance of this sample is possibly due to the presence of the rutile phase. It has been proposed that a smaller crystallite size and/or higher porosity result in improved electrochemical performance of titania [1,5,8,13]. However, A-NA and A-MK samples exhibited very similar crystallite sizes, and both crystallite size and APS of A-NA samples were smaller than those of A-SKS samples.

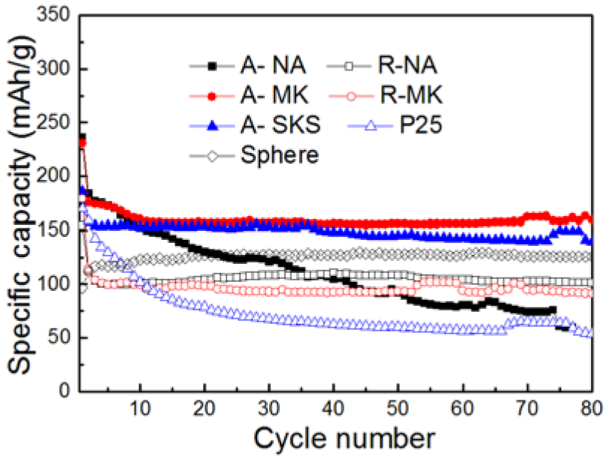

Figure 3. Cycling performance of LIB anodes based on different TiO_2 anodes at the discharge/charge rate is 100 mAh g^{-1}.

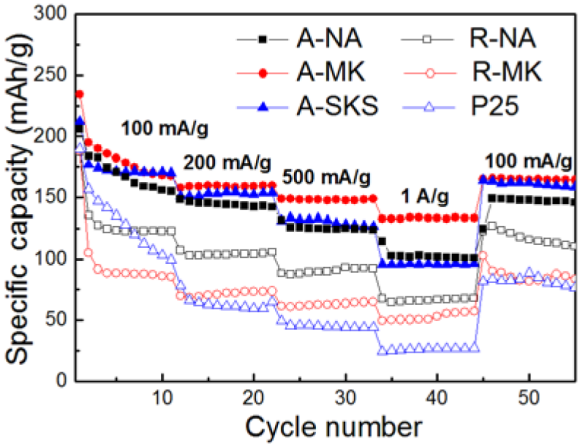

Figure 4. Rate cycle performance of different TiO_2 electrodes at charge/discharge rates from 100 mAh g^{-1} to 1 Ah g^{-1} for 55 cycles.

The specific capacities of rutile samples R-NA and R-MK are typically lower compared to anatase, as expected [1,4]. Their initial capacities differ (154 mA h/g for R-NA and 179 mA h/g for R-MK), but the specific capacities of 2 anodes remain within 2 mA h/g of each other for the first 20 cycles or so, and then the difference between them increases to ∼10 mA h/g by the 80th cycle (101 mA h/g for R-NA and 91 mA h/g for R-MK). On the other hand, R-NA exhibits an improved rate performance compared to R-MK, while the worst rate performance is observed for P25 sample, with specific capacity of only 27 mA h/g at the charge/discharge rate of 1 A/g. For this sample, there is also a significant drop in the specific capacity after the rate is reduced to 0.1 A/g (initially 99 mA h/g, reduced to 76 mA h/g). If we compare the crystallite sizes of R-NA and R-MK, we can observe that the crystallite size in R-MK is 2 times larger compared to R-NA. As already discussed, smaller crystallite size is expected to result in improved anode performance [1,5,8,13]. However, considering the large crystallite size difference and the small performance difference (in addition to the difference in morphologies and the presence of a small fraction of anatase phase), in combination with the fact that no strong correlation is observed between crystallite size and performance in the anatase sample, we can conclude that there are multiple factors affecting the performance of titania-based anodes and that a simple morphological and crystallographic

characterization is not sufficient to predict LIB performance of samples prepared by different methods (obtained from different commercial suppliers).

Finally, we also compared the LIB application performance between 2 mixed phase samples, P25 and titania spheres. While the initial capacity of the spheres is smaller (97 mA h/g compared to 170 mA h/g for P25), cycling performance of the spheres is excellent, with the specific capacity of 126 mA h/g at the 80th cycle, compared to 54 mA h/g for P25. This is likely due to the morphological advantages of porous structures for LIB applications [1,3,5]. Furthermore, the mesoporous titania spheres are expected to have a higher percentage of (001) facets [23]. Higher percentage of (001) facets compared to (101) is expected to result in a better reversibility of Li insertion/extraction [1].

To obtain more information about the material properties, Raman spectroscopy was used. The obtained results (for the excitation wavelength of 663 nm) are shown in Figure 5. Anatase crystals typically exhibit 6 Raman transitions located around 144 cm^{-1}, 197 cm^{-1}, 399 cm^{-1}, 515 cm^{-1}, 519 cm^{-1} (superimposed with the 515 cm^{-1} band), and 639 cm^{-1}, which can be ascribed to the E_g, E_g, B_{1g}, A_{1g}, B_{1g}, and E_g transition modes of the anatase phase, respectively [25,26]. Rutile crystals typically exhibit Raman transitions located at $\sim$143 cm^{-1}, 235 cm^{-1}, 447 cm^{-1}, and 612 cm^{-1}, which are assigned to B_{1g}, 2-photon scattering, E_g, and A_{1g}, respectively [26,27]. In the present study, 4 major Raman transition modes corresponding to the anatase

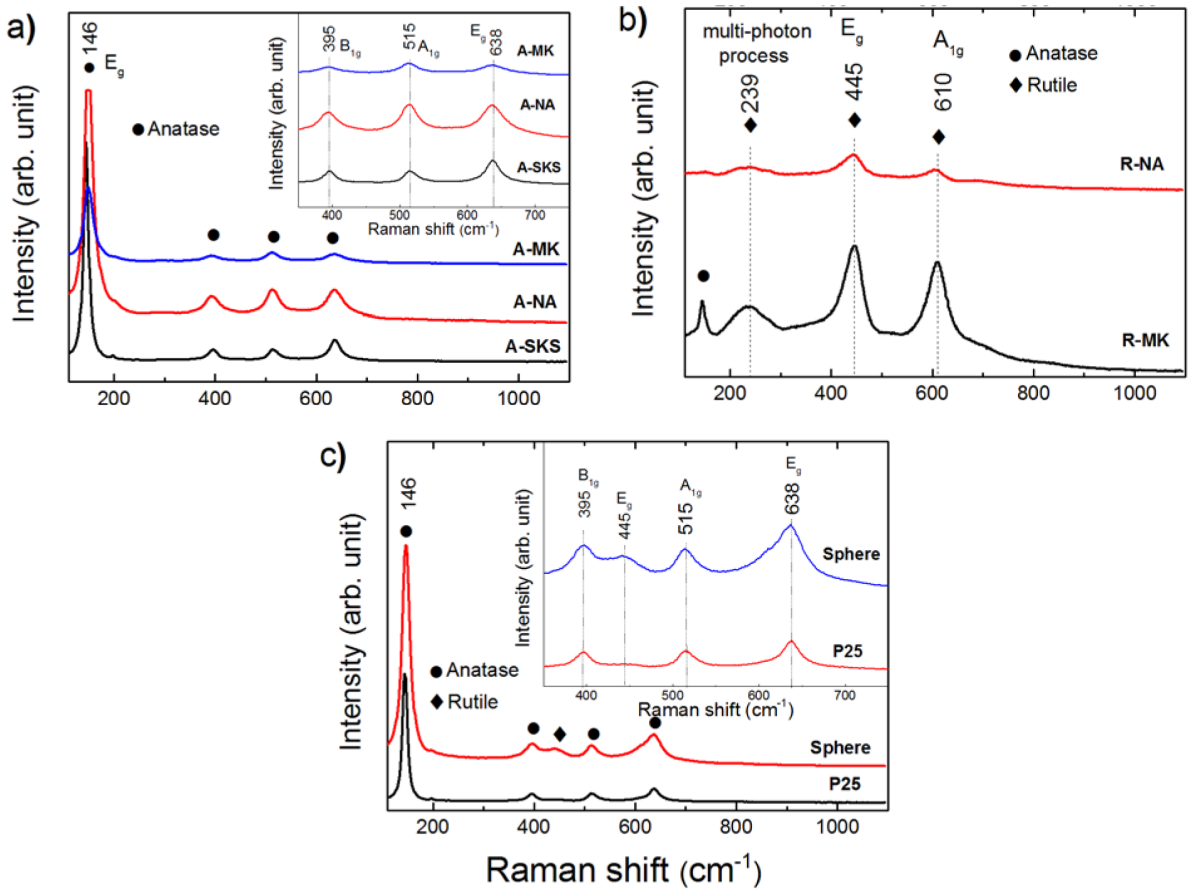

Figure 5. Raman spectra of different TiO_2 samples: (a) A-NA, A-MK, and A-SKS; (b) R-NA and R-MK; (c) P25 and TiO_2 microsphere.

crystal phase were observed for A-NA, A-MK, and A-SKS TiO_2: E_g (146 cm^{-1}), B_{1g} (395 cm^{-1}), A_{1g} (515 cm^{-1}), and E_g (638 cm^{-1}), as shown in Figure 5a. The Raman spectra of R-NA and R-MK are shown in Figure 5b. Three Raman modes were observed, attributed to a 2-photon process (239 cm^{-1}), E_g (445 cm^{-1}), and A_{1g} (610 cm^{-1}). In addition, for R-MK there is a weak transition mode at around 143 cm^{-1}. Since the band at 146 cm^{-1} is typically the strongest for the anatase phase, while the band around 143 cm^{-1} of rutile phase is the weakest one [26], this transition mode was likely due to the existence of anatase TiO_2 in the R-MK particles, consistent with the XRD results. Figure 5c shows the Raman spectra of P25 and sphere samples. The majority of the observed modes corresponded to those of the anatase crystal phase, although in the case of spheres a peak at around 445 cm^{-1}, attributed to the E_g Raman mode of the rutile phase [25], can also be clearly identified. Thus, the Raman spectroscopy results are consistent with the XRD data. We can also observe that the samples exhibiting better cycling performance also exhibit lower intensity of the Raman modes (A-MK compared to A-SKS and A-NA, as well as R-NA compared to R-MK). This is possibly due to the fact that more disordered structures are more likely having improved ability to buffer the volume changes upon lithium insertion/extraction and thus may exhibit improved retention of the specific capacity upon cycling. It should be noted that the same observation does not hold for the comparison between P25 and sphere samples, but these samples also exhibit a very large difference in the morphology and thus direct comparison is not appropriate despite similar crystal structures.

4. Conclusions

We have examined the properties and LIB anode performance of different titania samples. We found that the performance of different titania samples with the same crystal phase exhibits significant differences. The best performance observed for the pure anatase phase was better compared to the best performance observed for the rutile phase. The influence of the crystallite size does not appear to be the dominant factor affecting the LIB performance, while the presence of disorder may be an advantage for LIB applications. Finally, the micron-sized mesoporous structures exhibit improved performance compared to nanoparticle morphology.

Acknowledgments

Financial support from the Strategic Research Theme, University Development Fund, Seed Funding Grant (of the University of Hong Kong) is acknowledged. MHX would like to acknowledge the support of the Guangdong science and technology development plan (project No. 2010A090602002), while AMCN would like to acknowledge support from a grant from Shenzhen Science and Technology Commission (Project No. JCYJ20120830154526542).

References

[1] Jiang, C. H.; Zhang, J. S. *J. Mater. Sci. Technol.* **2013**, *29*, 97–122.

[2] Deng, D.; Kim, M. G.; Lee, J. Y.; Cho, J. Y.; Cho, J. *Energy Environ. Sci.* **2009**, *2*, 818–837.

[3] Weng, Z. Y.; Guo H.; Liu, X. M.; Wu, S. L.; Yeung, K. W. K.; Chu, P. K. *RSC Adv.* **2013**, *3*, 24758–24775.

[4] Fröschl, T.; Hörman U.; Kučerová, G.; Pfanzelt, M.; Weiss, C. K.; Behm, R. J.; Hüsing, N.; Landfester, K.; Wohlfahrt-Mehrens, M. *Chem. Soc. Rev.* **2012**, *41*, 5313–5360.

[5] Wang, H. E.; Jin, J.; Cai, Y.; Xu, J. M.; Chen, D. S.; Zheng, X. F.; Deng, Z.; Li, Y.; Bello, I.; Su. B. L. *J. Colloid Interface Sci.* **2013**, *417*, 144–151.

[6] Fernández-Werner, L.; Faccio R.; Juan, A.; Pardo, H.; Montenegro, B.; Mombrú, Á. W. *Appl. Surf. Sci.* **2014**, *290*, 180–187.

[7] Kong J.; Wei, Y. F.; Zhao, C. Y.; Toh, M. Y.; Yee, W. A.; Zhou, D.; Phua, S. L.; Dong, Y. L.; Lu, X. H. *Nanoscale* **2014**, *6*, 4352–4360.

[8] Charette, K; Zhu, J.; Sally, S. O.; Ng, K. Y.; Deng, D. *RSC Adv.* **2014**, *4*, 2557–2562.

[9] Singh, D. P.; George, A.; Kumar, R. V.; ten Elshof, J. E.; Wagemaker, M. *J. Phys. Chem. C* **2013**, *117*, 19809–19815.

[10] Chen, J. S.; Liang, Y. N.; Li, Y. M.; Yan, Q. Y.; Hu, X. *ACS Appl. Mater. Interfaces* **2013**, *5*, 9998–10003.

[11] Hao, B.; Yan, Y.; Wang, X. B.; Chen, G. *ACS Appl. Mater. Interface* **2013**, *5*, 6285–6291.

[12] Tao, T.; Chen, Y. *Mater. Lett.* **2013**, *98*, 112–115.

[13] Rai, A. K.; Anh, L. T.; Gim, J. H.; Mathew, V.; Kang, J. W.; Paul, B. B.; Song, J. J.; Kim, J. *Electrochim. Acta* **2013**, *90*, 112–118.

[14] Shen, J. Y.; Wang, H.; Zhou, Y.; Ye, N. Q.; Li, G. B.; Wang, L. J. *RSC Adv.* **2012**, *2*, 9173–9178.

[15] Hardwick, L. J.; Holzapfel, M.; Novák, P.; Dupont, L.; Baudrin, E. *Electrochimica Acta* **2007**, *52*, 5357–5367.

[16] Wang, Z. Y.; Lou, X. W. *Adv. Mater.* **2012**, *24*, 4124–4129.

[17] Wang, J.; Zhou, Y. K.; Hu, Y. Y.; O'Hayre, R.; Shao, Z. P. *J. Phys. Chem.* C **2011**, *115*, 2529–2536.

[18] Liu, S. H.; Wang, Z. Y.; Yu, C.; Wu, H. B.; Wang, G.; Dong, Q.; Qiu, J. S.; Eychmüller, A.; Lou, X. W. *Adv. Mater.* **2013**, *25*, 3462–3467.

[19] Yildirim, H.; Greeley, J. P.; Sankaranarayannan, S. K. R. S. *J. Phys. Chem. C* **2013**, *117*, 3834–3845.

[20] Ban, C. M.; Xie, M.; Sun, X.; Travis, J. J.; Wang, G. K.; Sun, H. T.; Dillon, A. C.; Lian, J.; George, S. M. *Nanotechnology* **2013**, *24*, 424004.

[21] Hwa, Y.; Kim, W.-S.; Yu, B.-C.; Kim, J.-H.; Hong, S.-H.; Sohn, H.-J. *J. Electroanal. Chem.* **2014**, *712*, 202–206.

[22] Wang, W. S.; Sa, Q. N.; Chen, J. H.; Wang, Y.; Jung, H. J.; Yin, Y. D. *ACS Appl. Mater. Interfaces* **2013**, *5*, 6478–6483.

[23] Zhao, Z.; Sun, Z. C.; Zhao, H. F.; Zheng, M.; Du, P.; Zhao, J. L.; Fan, H. Y. *J. Mater. Chem.* **2012**, *22*, 21965–21971.

[24] Djerdj, I.; Tonejc, A. M. *J. Alloys Compd.* **2006**, *413*, 159–174.

[25] Chen, C. A.; Huang, Y. S.; Chung, W. H.; Tsai, D. S.; Tiong, K. K. *J. Mater. Sci: Mater. Electron* **2009**, *20*, S303–S306.

[26] Zhang, J.; Li, M. J.; Feng, Z. C.; Chen, J.; Li, C. *J. Phys. Chem. B* **2006**, *110*, 927–935.

[27] Yan, J. Q.; Wu, G. J.; Guan, N. J.; Li, L. D.; Li, Z. X.; Cao, X. Z. *Phys. Chem. Chem. Phys.* **2013**, *15*, 10978–10988.